applied sciences

MDPI

Article

Parametric Optimization of System Modes for Nozzle Turbine Vane by Means of Costimulated Artificial Immune System

Rafał Robak [1,*], Mirosław Szczepanik [2] and Sebastian Rulik [3]

[1] AvioPolska Sp. z o.o., Michała Grażyńskiego 141, 43-346 Bielsko-Biała, Poland
[2] Faculty of Mechanical Engineering, Silesian University of Technology, Konarskiego 18A, 44-100 Gliwice, Poland; miroslaw.szczepanik@polsl.pl
[3] Faculty of Energy and Environmental Engineering, Silesian University of Technology, Konarskiego 18, 44-100 Gliwice, Poland; sebastian.rulik@polsl.pl
* Correspondence: rafal.robak@avioaero.it; Tel.: +48-885-206-601

Featured Application: Parametric optimization design study of low-pressure turbine vane by means of artificial immune system.

Abstract: One requirement posed by customers is to achieve adequate durability levels as described in technical requirement documents. Modal analysis is one of the design assessments aimed at identifying the risks of high cycle fatigue (HCF). This article presents a novel application of an artificial immune system (AIS) in the optimization of a nozzle guide vane's modal characteristics. The aim is to optimize the system's natural frequencies in the vibration vane and adjacent hardware (turbine casing). The geometrical characteristics accounted for in the optimization process include the shell thicknesses on the turbine casing side and the nozzle outer band features (hook thickness, leaning and position). The optimization process is based on a representative model established from FEM analysis results. The framework is robust because of the applied metamodel and does not require time-consuming FEM analysis in order to evaluate the fitness function. The aim is to minimize the model area (a derivative of the system weight) with constraints imposed on the frequency (a penalty function). The optimum design is given as the solution with an increased shell thickness in the turbine casing and leaning nozzle outer band hooks to obtain the maximum stiffness of the system. The results obtained by means of the artificial immune system (AIS) and a novel variant based on an additional costimulation procedure (CAIS) are compared with the solution obtained by means of a genetic algorithm implemented in the commercial CAE software (Ansys version 19.2).

Keywords: modal analysis; vane; artificial immune system; optimization; system mode

Citation: Robak, R.; Szczepanik, M.; Rulik, S. Parametric Optimization of System Modes for Nozzle Turbine Vane by Means of Costimulated Artificial Immune System. *Appl. Sci.* **2024**, *14*, 3991. https://doi.org/10.3390/app14103991

Academic Editors: José António Correia and Wei Huang

Received: 17 March 2024
Revised: 12 April 2024
Accepted: 28 April 2024
Published: 8 May 2024

1. Introduction

A balance between program requirements like weight or durability and component costs is crucial to create competitive products. The design process of nozzle vanes (Figure 1) includes a modal analysis [1,2].

The results of the modal analysis are the modal forms (eigenvectors) and associated natural frequencies (eigenvalues) of the system. This analysis is crucial to understand the dynamic behavior and avoid failure modes related to high cycle phenomena. The development phase extensively uses finite element method (FEM) analyses [3]. The reported approach is based on a metamodel established via 2D modal analysis. A surrogate model describes the relationship between the geometrical characteristics and the natural frequency and model area. Typically, an optimization process on airfoils is used to tune the performance [4], lift coefficient [5] and turbine blade aerodynamics [6]. Blade natural frequency optimization [7] accounts for the thickness as a geometrical characteristic. The study presented in [8] revealed the additional impacts of the thicknesses, hook positions and leaning on the casing nozzle assembly.

Figure 1. Nozzle guide vane of low-pressure turbine in aircraft engine.

In the optimization process, an artificial immune system and a novel version of the algorithm based on costimulation were used. The use of artificial intelligence methods in the optimization of engineering problems is becoming more and more common. The combination of artificial intelligence methods with algorithms in the numerical analysis of engineering problems, such as the finite element method, makes it possible to obtain effective tools to support the work of an engineer. Examples of the use of artificial intelligence in various technical problems are considered in [9–11].

The nozzle geometry can be subdivided into several design zones, as presented in Figure 2. The primary criterion for zone A (aerodynamic profile) is to meet the requirements regarding the turbine performance and flow function through airfoil design. A secondary aspect in this location is related to the dynamic characteristics of the airfoil. Location B is the connection between the airfoil and the outer and inner bands. This zone is mainly optimized for the level of stress in order to maximize the components' durability. An example of such a study is presented in [12]. Zone D establishes proper sealing between the rotating components (bladed disks and interstage seals) and prevents hot gas from bypassing the main flow path (reducing the performance). Zone C is designed to ensure correct mounting with the casing rails; it is determined by the durability requirements and is the subject of the optimization.

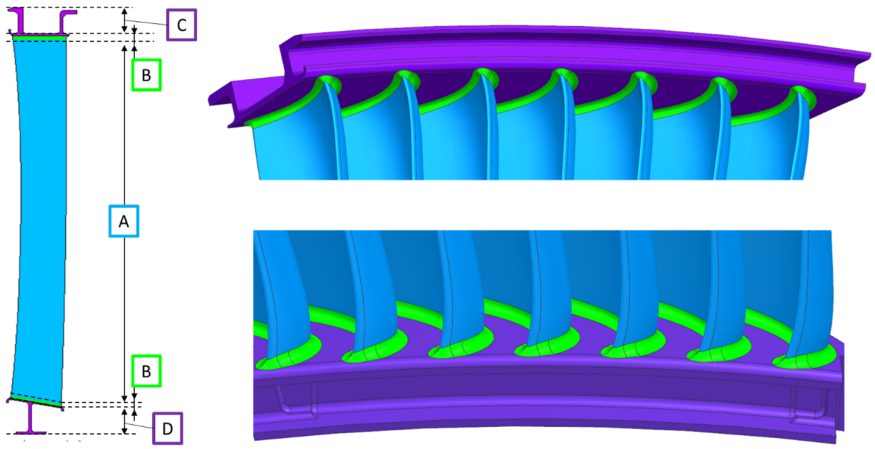

Figure 2. Nozzle guide vane—design zones; A—aerodynamic profile, B—hub and tip fillets, C—outer band, D—inner band.

Typical failure modes for nozzle guide vanes are low cycle fatigue (LCF), high cycle fatigue (HCF), creep and environmental attack (oxidation and corrosion). The main contributors to the low and high cycle fatigue failure modes are thermal and pressure

loads. A thermal load creates thermal stress due to the gradients between the aerodynamic profile and the inner and outer bands. A pressure load pushes the nozzle backward, which concentrates the stresses at the airfoil tip and outer band hooks (the simple supported beam concept). The HCF failure mode relates to the vibration of the structure due to excitation of a natural frequency within the operating range (high dynamic response; see Figure 3).

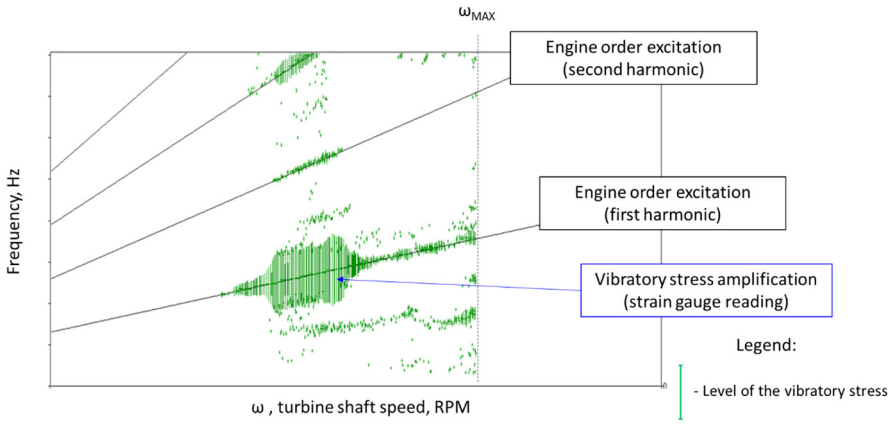

Figure 3. Experimental Campbell diagram with noticeable dynamic response of the nozzle.

2. Materials and Methods

2.1. Formulation of the Optimization Function

For the optimization of the dynamic characteristics, the function J_0 and a set of constraints (related to frequency level O_1 and the design variable domain) are defined. The optimization problem can be described as a set of design variables (1) for which the optimization function (2) reaches a global minimum.

$$X = [x_1, x_2 \ldots x_i \ldots x_n], \tag{1}$$

where:

n—number of design variables (geometrical parameters);
x_i—ith design variable from design domain $[x_i]_{MIN} < x_i < [x_i]_{MAX}$,

$$\min_X J_0(X), \tag{2}$$

where:

J_0—optimization function;
X—design variable vector.

The desired frequency level of the nozzle guide vane system is driven by the Campbell diagram, presented in Figure 4. The aim is to reach a natural frequency above the excitation level coming from rotor imbalance.

$$O_1 \rightarrow f_1 \geq 125 \text{ Hz}, \tag{3}$$

where: f_1—natural frequency of the nozzle guide vane, i.e., the first system mode.

The optimization function used in this work is described by Equation (4), including a penalty formula due to the constraint imposed on the frequency:

$$J_0 = \int_\Omega d\Omega * \gamma_{freq} \rightarrow \min_{X_A} J_0(X_A), \tag{4}$$

where:

Ω—model area;

X_A—set of geometrical design variables;
γ_{freq}—penalty function defined according to constraint O_1.

The penalty function is represented by Equation (5):

$$\gamma_{freq} = \begin{cases} If\ f_1 < 125\ then\ (125 - f_1) * 2 \\ else\ 1 \end{cases}. \quad (5)$$

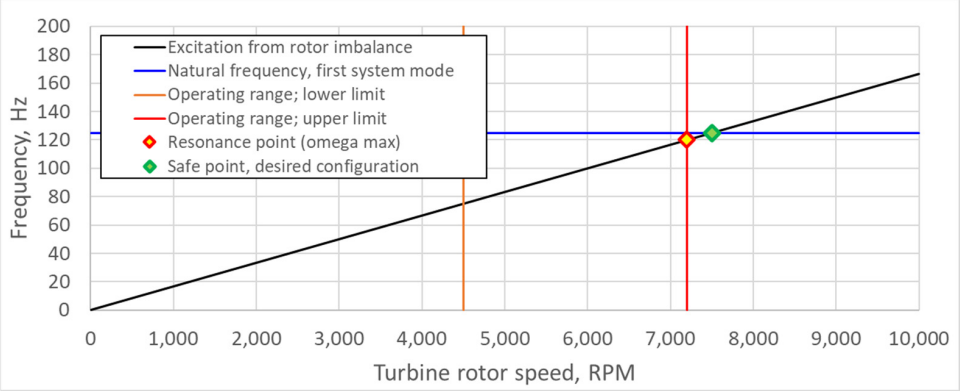

Figure 4. Campbell diagram—O1 constraint definition (green point).

In the next section, the design parameters and optimization algorithm used to solve the defined optimization problem are described.

2.2. Artificial Immune System with Costimulation Effect

Immunology [13] describes the biological and biochemical processes of the immune system in reaction to pathogens or external substances like toxins. The immune system is characterized by the fuzzy detection of anomalies and self-organization. The system is composed of multilayer barriers and each of the elements has a different strategy and defense mechanism. The first two fundamental layers are the skin (a mechanical barrier protecting from biological, chemical and other physical factors) and physiological barrier (the body's temperature, pH level). The third layer of the system is the inborn immune system, which is not subjected to any changes during life. The most interesting from an artificial intelligence standpoint is the fourth layer, called the adaptive defense immune system. This layer is able to design an immune response to particular pathogens through continuous learning. The main actors in this system are B-lymphocytes (B-cells), presented in Figure 5, and T-lymphocytes (T-cells).

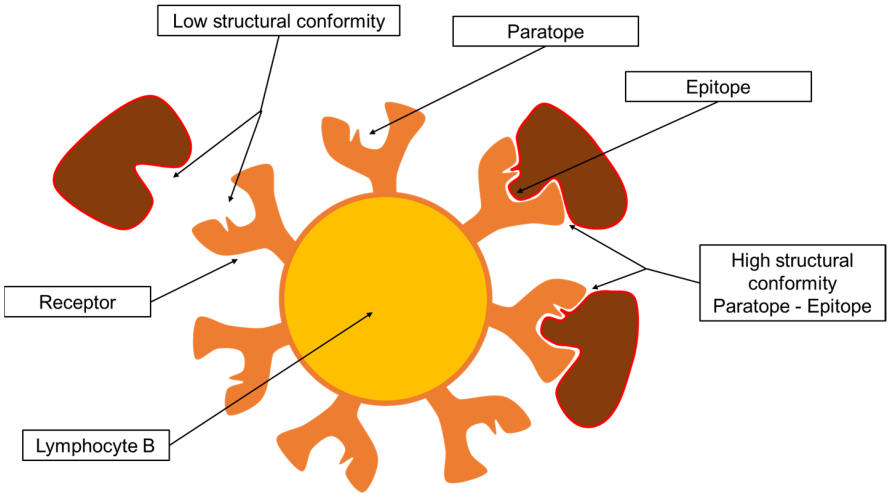

Figure 5. B-lymphocyte (B-cell) notional scheme.

The basic pathogen detection mechanism is to use the high structural conformity between the paratope of the lymphocyte and the epitope of the pathogen. This concept was used as the foundation for the artificial immune system algorithm defined in [14]. The optimization strategy assumes a pathogen as the optimal solution and finds the best B-cell (design configuration) to match this pathogen. The main steps of the algorithm are described in Figure 6.

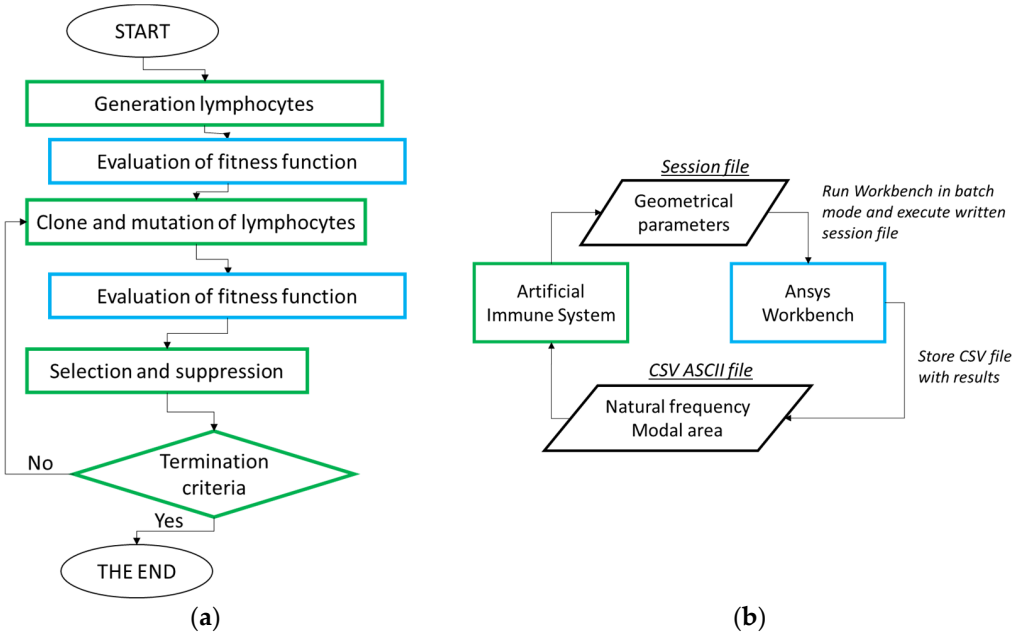

Figure 6. Artificial immune system (AIS): (**a**) flowchart of optimization algorithm, (**b**) data management.

The first step of the algorithm is to generate and initialize B-lymphocytes that represent different geometrical design configurations. In the present work, such initialization is based on a randomized approach in the defined domain. In the next step, the fitness function is evaluated, representing the structural conformity between the lymphocyte (paratope) and pathogen (epitope).

$$L_B(t) = \left[L_{B_t}^1,\ L_{B_t}^2,\ \ldots, L_{B_t}^j, \ldots, L_{B_t}^N\right], \tag{6}$$

where:

t—iteration index (population);
j—number of B-cells;
N—number of B-cells in the population;
$L_{B_t}^j$—j-th B-cell in population t,

$$L_{B_t}^j = \left[x_1^j, x_2^j, \ldots, x_i^j, \ldots, x_n^j\right], \tag{7}$$

where:

n—number of paratopes in the B-lymphocyte;
x_i^j—i-th paratope in the j-th B-lymphocyte.

The main section of the algorithm responsible for the exploration and exploitation of the design domain is the cloning and mutation procedure. The applied variable schemes follow biological processes. Cloning is proportional to the fitness function result, as reported in Equation (8).

$$C_j = \frac{C}{L_{RANK}}, \tag{8}$$

where:

C_j—number of clones of j-th B-cell;
C—number of clones defined as algorithm parameter;
L_{RANK}—lymphocyte rank basing on the fitness function result: $1, 2, 3, \ldots, L_N$;
L_N—number of B-cells defined as algorithm parameter.

The mutation procedure, by contrast, uses the fitness function result and lymphocyte rank to apply an inverse proportional rule. A better B-cell has a lower value of the mutation coefficient to obtain convergence.

$$m_j = m * \frac{L_{RANK}}{L_N}, \tag{9}$$

where:

m_j—mutation coefficient for j-th B-lymphocyte;
m—mutation coefficient.

A summary of the mutation procedure for clone $CL_B(t)$ is given in Equation (10).

$$\forall x^{*j}_i = x^j_i + m_j RND(-1,1)\left(x^{UL}_i - x^{LL}_i\right), \tag{10}$$

where:

$RND(-1,1)$—random number from -1 to 1 with uniform probability;
x^{LL}_i—lower range for design parameter x_i;
x^{UL}_i—upper range for design parameter x_i.

Each clone is assessed against the fitness function and the algorithm proceeds to the final step related to selection and suppression. A fixed number of B-cells is one of the algorithm parameters; therefore, at the end of each iteration, some of clones need to be rejected. This process is performed with a direct back-to-back comparison between the B-cell and a B-cell clone. If the clone shows a better fitness function, it replaces the B-cell for the next iteration. Additionally, as described in the literature [14], the applied congestion coefficient aims to maintain continuous domain exploration. If parameter r defined in Equation (11) is less than the defined threshold, the lymphocyte with the lower fitness function is replaced by a randomly generated new lymphocyte.

$$r = \sqrt{\sum_{i=1}^{n} \frac{\left(x^j_i - x^{j+1}_i\right)^2}{\left(x^{UL}_i - x^{LL}_i\right)^2}}, \tag{11}$$

where:

r—distance between lymphocytes (memory cells).

Before the next iteration, the algorithm verifies the termination criteria. Artificial immune systems are used in the solution of various engineering problems, as reported in [15,16].

A more complex optimization strategy, as presented in this work, is the concept of a costimulated artificial immune system (CAIS). The biological mechanism is described in Figure 7.

The B-lymphocyte (B-cell) is activated—it is transformed into a lymphoblast only in the case of additional stimulation from a T-lymphocyte (T-cell). The method of activation depends on the recognition of a B-cell that presents an antigen to a T-cell through the major histocompatibility complex (MHC) peptide. If the T-cell recognizes the antigen, it produces interleukins, which starts the lymphoblast reaction and proliferation phase. The lymphoblasts (activated lymphocytes) produce antibodies against the recognized pathogen and this is part of the immunological reaction. In time, the lymphoblasts are back-transformed into B-cells and some of them remain as plasma cells ready to produce antibodies in the future to support memory reactions. If the B-cell at the first step does

not receive positive stimulation from a T-cell, then it will be removed from the body, as presented in Figure 8. This mechanism prevents autoimmunological diseases in the body.

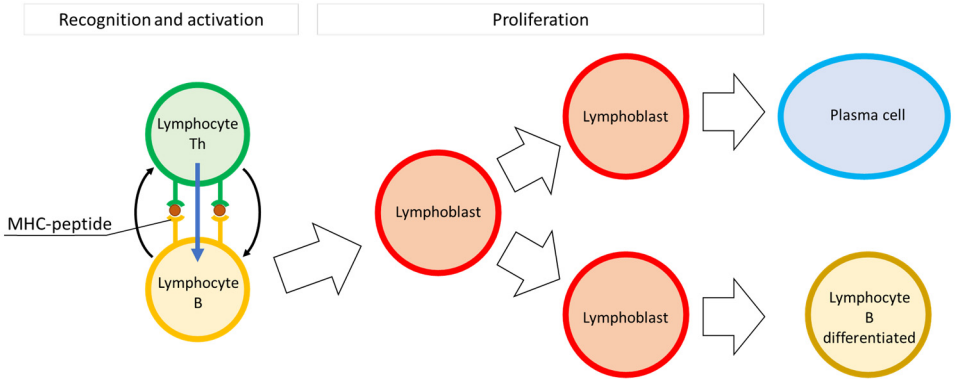

Figure 7. Costimulation effect between B- and T-lymphocytes.

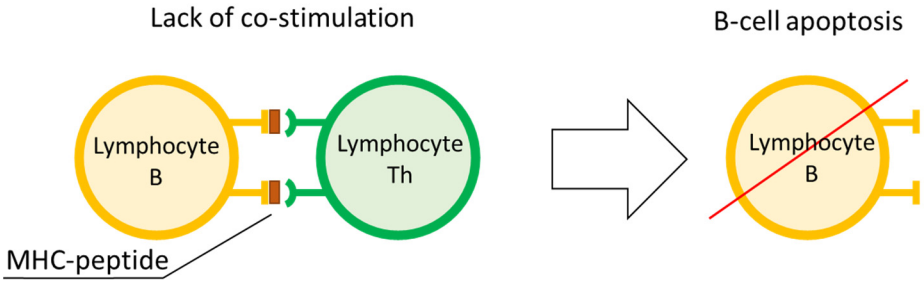

Figure 8. Costimulation impact on B-lymphocyte.

The adaptation of the presented scheme into an optimization strategy is reported in Figure 9. The costimulation element is incorporated in order to assess a particular design configuration in the optimization loop (represented by a B-cell) by a metamodel (represented by a T-cell). The surrogate model (second-order polynomial function) is established on a database of previously calculated design points. The main motivation for the implementation of this mechanism is to collect information from each fitness function evaluation in the database and use these data for the result prediction. Costimulation is the rejection of less promising geometrical configurations, reducing the number of analyses needed.

The CAIS requires an additional parameter to manage the representation of the T-lymphocytes (reported in Table 1). The aim of the additional factor is to determine how often the metamodel (T-cell representation) needs to be refreshed and to apply a margin for the costimulation predictor (a decision point for the design configuration).

Table 1. Parameters of the CAIS: T-cell.

Parameter	Value
Frequency of T-cell refresh, fitness function evaluations	20
T-cell margin for criterion O1	5%

The presented approach (CAIS) was verified using test functions and compared with a standard artificial immune system (AIS). The results are presented in Figure 10. The performance of the algorithm was assessed taking into consideration the convergence to a global minimum and the number of fitness function evaluations.

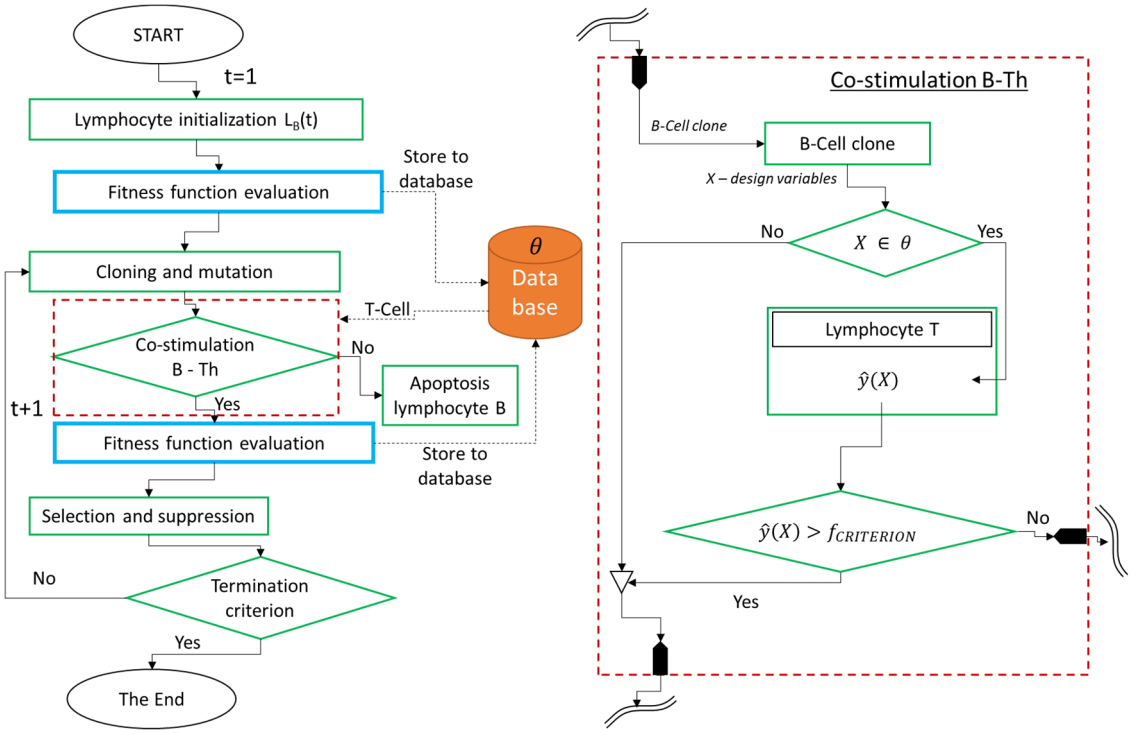

Figure 9. Costimulated artificial immune system (CAIS).

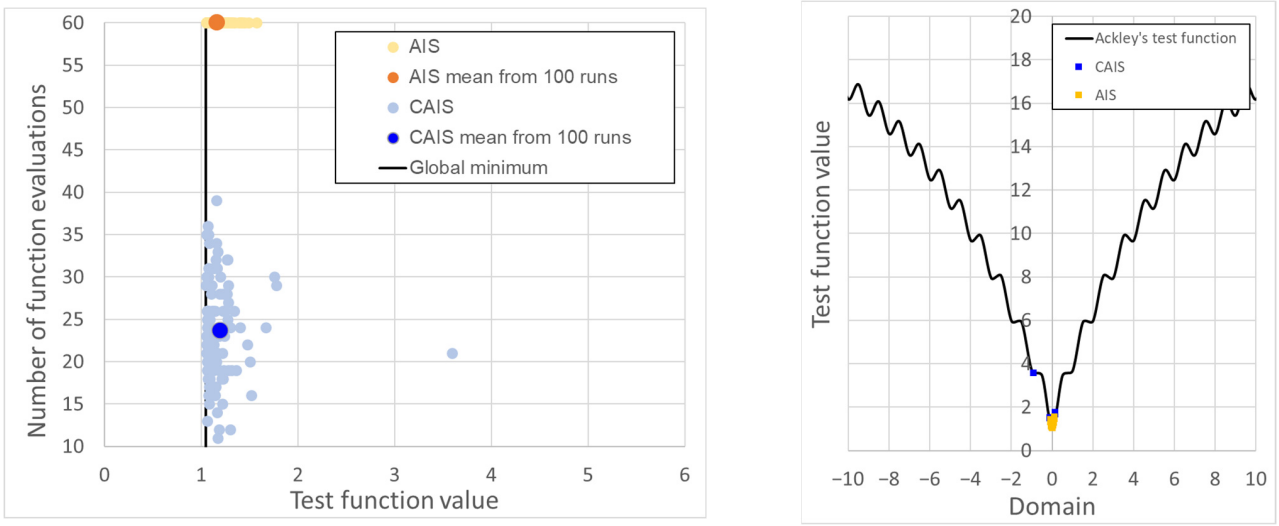

Figure 10. Ackley's function—comparison of standard artificial immune system (AIS) with costimulated artificial immune system (CAIS).

The Ackley test function is described by expression (12), where the global minimum is equal to 1.051 for $x = 0$.

$$f(x) = -20e^{-0.2\sqrt{0.5x^2}} - e^{0.5cos\pi x} + e + 20, \quad (12)$$

The algorithm parameters used in the comparative study are reported in Table 2.

The minimalization task of the test function was run 100 times in the standard and costimulated variants. As reported in the Table 2, the number of iterations was set to 10 and three memory cells were applied. The comparison of the average values from 100 runs showed a 61% lower number of fitness function evaluations for the CAIS than for

the AIS. At the same time, the reached minimum was only 3% worse with respect to the standard algorithm.

Table 2. Algorithm parameters.

Parameter	Value
Memory cells	3
Clone number	6
Termination criteria—number of iterations	10
Mutation probability	0.75

The next test function used in the comparative assessment was the Bohachevsky function, described by Equation (13), with a global minimum for $x = 0, f(x) = 0$.

$$f(x) = x^2 - 0.3cos(3\ \pi\ x) + 0.3, \quad (13)$$

The parameters used in the study were the same and are reported in Table 2. Figure 11 reports the results and the comparison of the two algorithms.

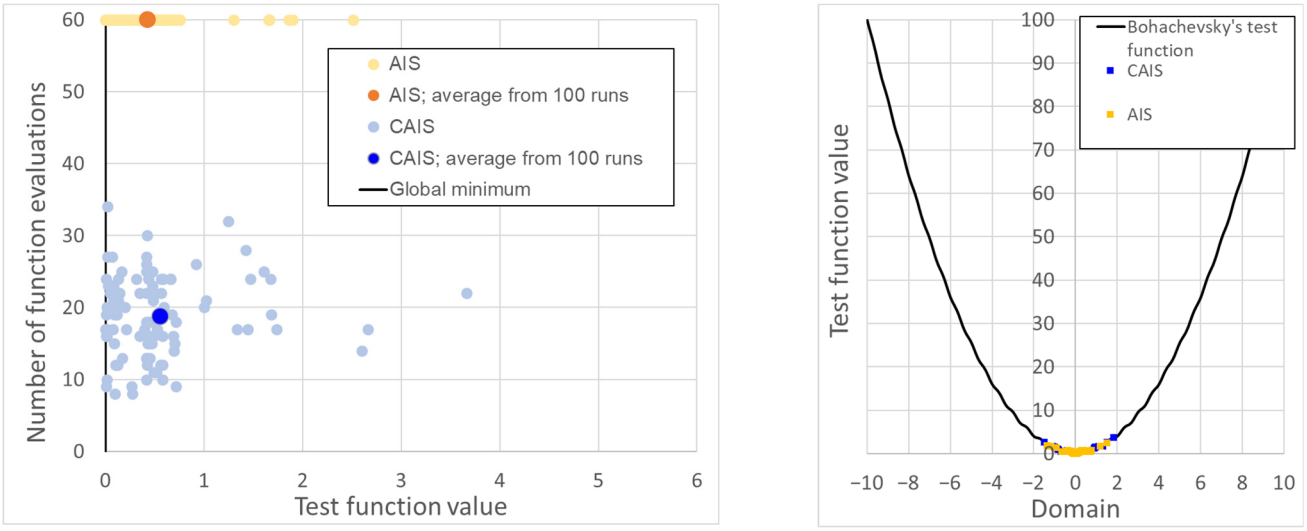

Figure 11. Bohachevsky's function—comparison of standard artificial immune system (AIS) with costimulated artificial immune system (CAIS).

Similarly, the optimization task was run 100 times for both algorithms: AIS and CAIS. The outcomes remained the same. Comparing the averaged values of the reached minimum, the AIS showed better results than the CAIS—in this particular case, by 29%. The CAIS, however, required a lower number of function evaluations, by 69% on average.

In summary, the standard artificial immune system shows better convergence to a global minimum based on the analyzed test functions; however, the costimulated algorithm shows better effectiveness (less computational effort). This result is directly translated into a shorter optimization lead time that is required in the component design phase (in the case of real industrial problems).

2.3. FEM Model Description and Optimization Framework

An analysis based on a simplified two-dimensional model of a vane with casing is performed. The nozzle guide vane is modeled by means of plane stress with thickness elements. The casing is modeled by means of axisymmetric elements. Appropriate thicknesses are established based on the perimeters derived from the radius of the area's center of gravity (CoG), as reported in Figure 12. The aerodynamic profile was additionally scaled based on the empty to full volume ratio.

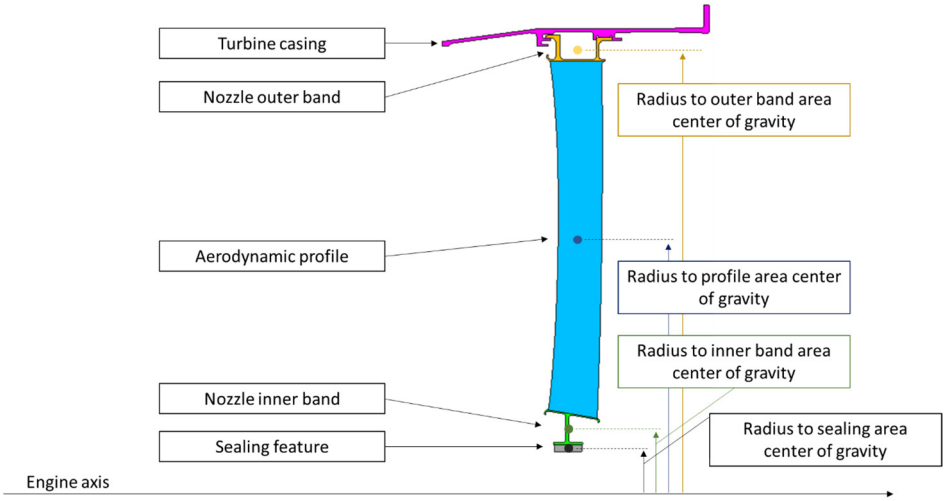

Figure 12. Approach for two-dimensional analysis.

The FEM model is subdivided into different areas to reflect the different behavior (axisymmetric and plane stress) and model thickness. These areas are merged by means of contact elements defined as presented in Figure 13.

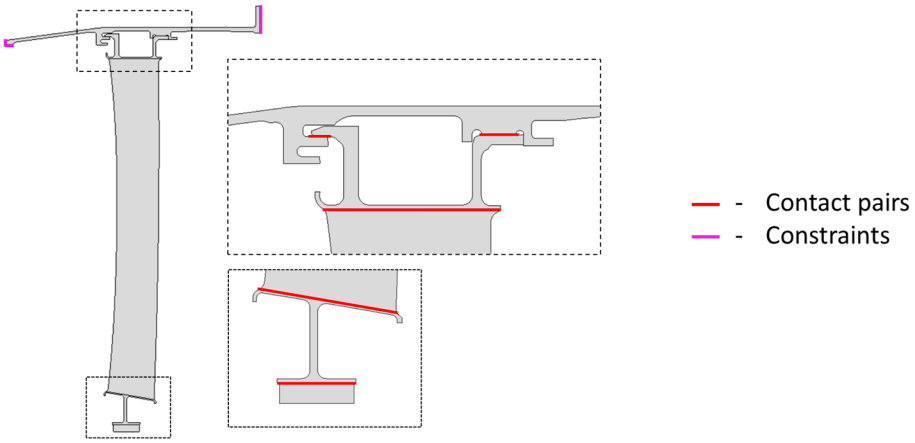

Figure 13. FEM model constraints and contact pair definition.

The defined contacts restrain relative movement and guarantee the absence of separation between the surfaces. The turbine casing is fixed in the radial and axial directions on the forward cut face and rear flange. The temperature of the casing and nozzle is set to ambient temperature.

The parameters for the optimization process are defined based on the strain energy distribution for the first system mode in the baseline (reference) configuration. Figure 14 highlights the zones with energy accumulation due to the considered mode shape deformation. A change in the stiffness in the highlighted zone will impact the natural mode frequency and therefore qualitatively defines the area of interest for parameterization.

A parametric model is defined by the casing shell thicknesses and the nozzle outer band hook's geometrical characteristics, as presented in Figure 15. The parameters related to the hook position and leaning also affect the casing geometry due to the need for casing rail adjustment (the rails follow the hook to ensure a contact interface).

Tables 3 and 4 define the lower and upper bounds of the geometrical characteristics applied in the optimization.

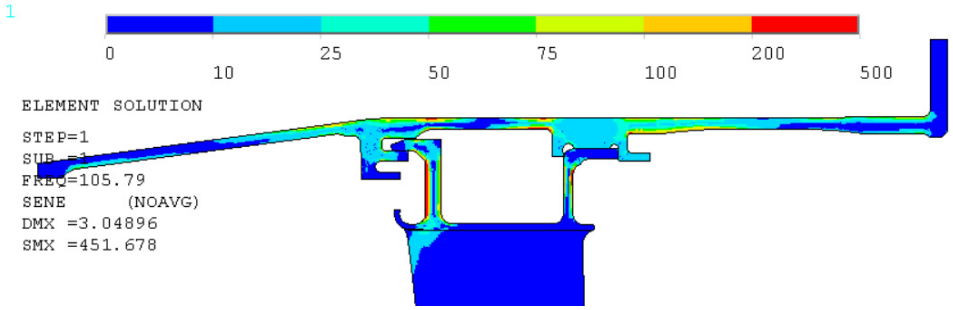

Figure 14. Strain energy distribution for pendulum mode shape.

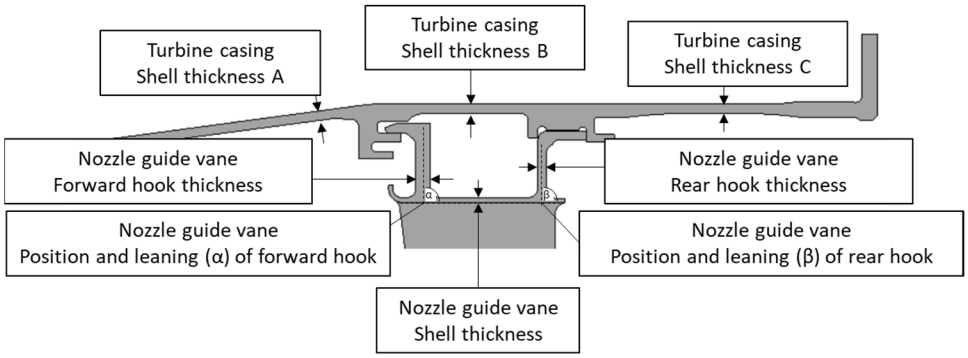

Figure 15. Geometrical parameters dedicated to optimization.

Table 3. Geometrical thickness and position parameters.

Parameter	Lower Bound, in	Upper Bound, in
Casing shell A	0.080	0.120
Casing shell B	0.080	0.180
Casing shell C	0.080	0.120
Forward hook thickness	0.100	0.200
Rear hook thickness	0.090	0.120
Nozzle shell thickness	0.060	0.120
Forward hook position	−0.040	0.040
Rear hook position	−0.050	0.050

Table 4. Geometrical angular parameters.

Parameter	Lower Bound, deg.	Upper Bound, deg.
Forward hook leaning	80	100
Rear hook leaning	80	100

The characteristic of the first system mode is presented in Figure 16. The nozzle is moving as a pendulum (an inner band traveling back and forth), being bonded to the turbine casing. The second and the following system modes of the structure are not within the scope of interest since they are outside the operating range and are not in interaction with any excitation source from shaft imbalance.

The optimization process is performed by means of an artificial immune system with the framework presented in Figure 17 (green box item represents optimization algorithm routine, blue box items identify CAE software operations). The process starts with the definition of a parametric model considering the set of geometrical characteristics selected from the strain energy distribution. The model is verified to ensure the geometry's feasibility within the established design variable ranges (Tables 3 and 4).

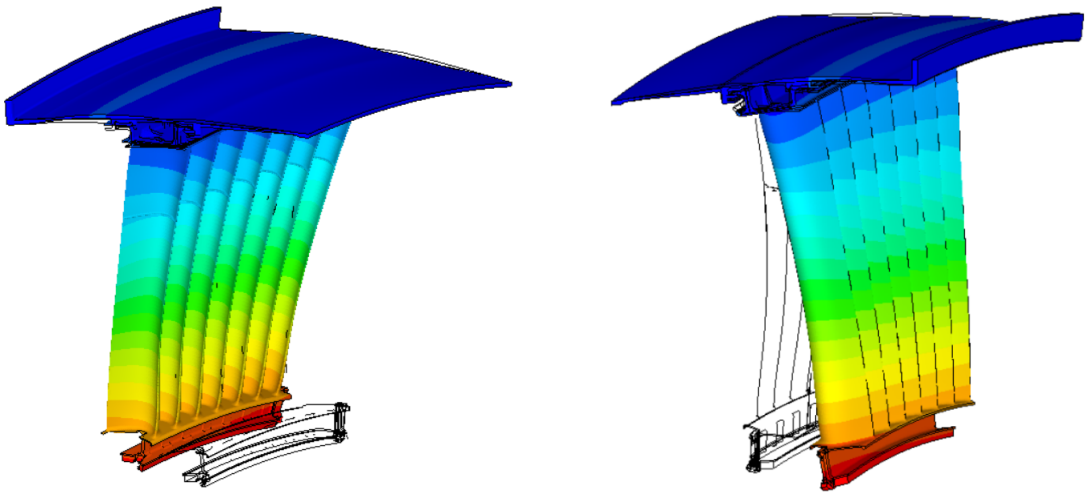

Figure 16. First system mode of nozzle guide vane—pendulum mode shape.

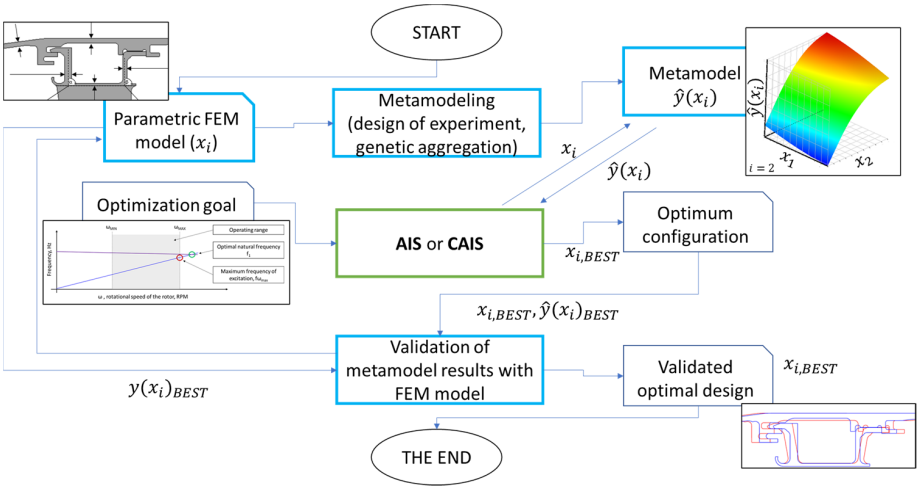

Figure 17. Optimization framework.

The optimization loop uses a static metamodel [8] that is an approximation of the real phenomena concerning the model area and natural frequency. The algorithm is responsible for design space exploration, while the Ansys Workbench environment [15] is used to extract the natural frequency and mode shape of the geometrical configuration. At the end of the process, the obtained result on the metamodel is validated with the FEM results to confirm the mathematical model's prediction.

The above framework was applied with the classical artificial immune system and with the costimulated variant. The results are compared in the next section.

3. Results

In the optimization process, the AIS algorithm with the parameters described in Table 5 was applied.

Table 5. Algorithm parameters.

Parameter	Value
Lymphocyte number (memory cells)	3
Clone number	6
Termination criteria, iteration quantity	40
Probability of mutation	0.75
Number of design variables	10

The model area change is presented in Figure 18 for three lymphocytes (memory cells). In the chart, two separate phases can be distinguished. The first phase is aimed to increase the model area and the system stiffness in order to meet the natural frequency criterion. Lymphocyte B_1 reached the natural frequency threshold at iteration 9, lymphocyte B_2 at iteration 14 and lymphocyte B_3 at iteration 16. In the second phase, the algorithm reduces the model area while keeping the natural frequency above 125 Hz (optimization constraint) (see Figure 19).

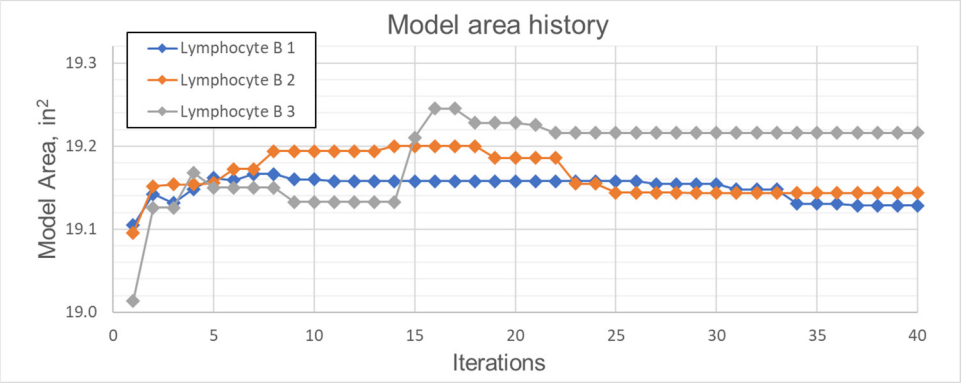

Figure 18. The change in model area—history.

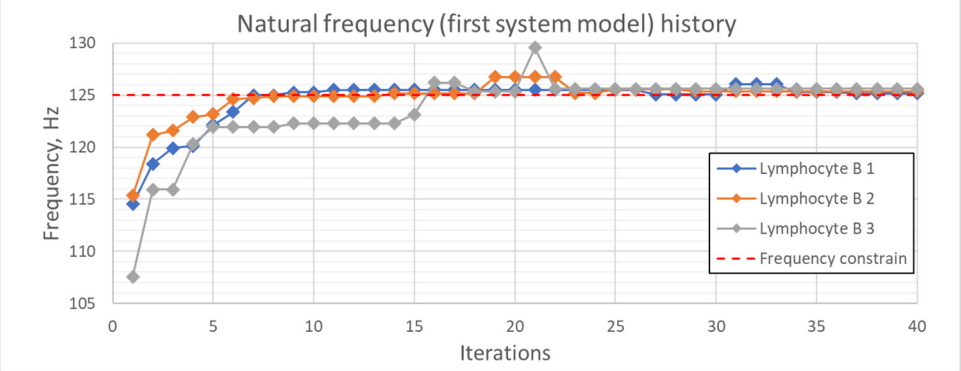

Figure 19. The change in natural frequency—history.

The memory cell is replaced by a clone if it is better than the current lymphocyte (representing the design variant). Note that a change does not occur in every iteration.

The algorithm completed 40 iterations and performed an evaluation through the metamodel 443 times. The convergence history for the averaged model area and the frequency results are presented in Figure 20.

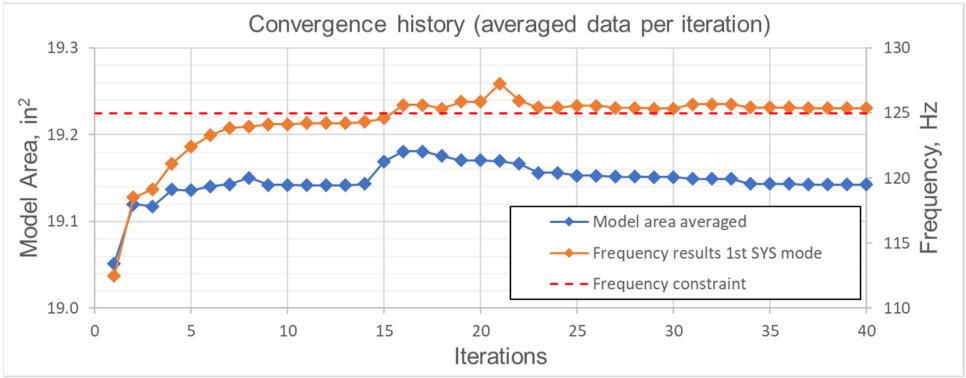

Figure 20. The convergence history—averaged results.

Figure 21 shows the change in the standard deviation of the memory cells during the iterations. The data for the natural frequency's standard deviation revealed a reduction in spread due to the applied constraint.

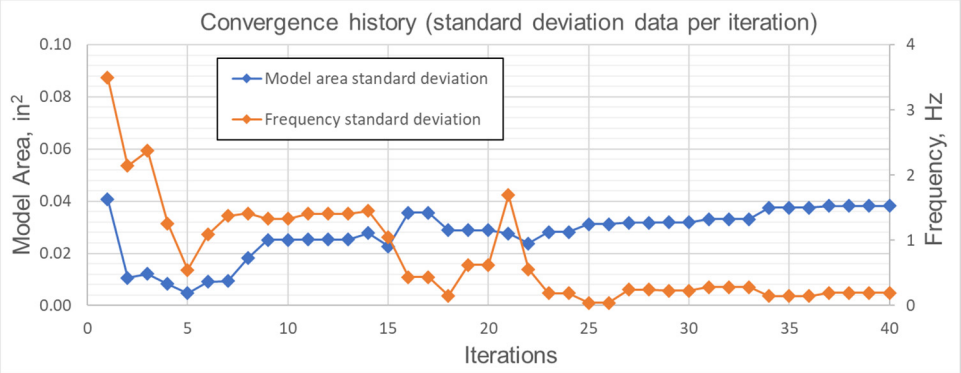

Figure 21. Convergence history (averaged data per iteration).

A comparison of the best obtained configuration with the reference one is presented in Figure 22. The reference model is a preliminary design configuration established on a legacy low-pressure turbine nozzle design. The main changes observed are related to the turbine case shell thickness (impacting both the frequency and model area) and the hook leaning and position.

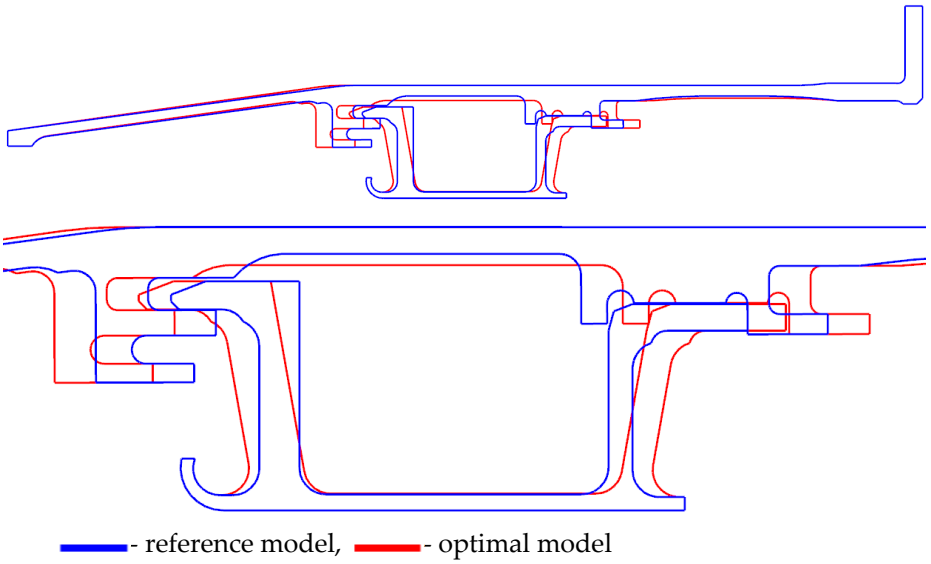

Figure 22. Optimum design geometry—comparison with reference model.

The same study was performed by means of a commercially incorporated genetic algorithm (GA). Table 6 reports the design variable values reached for the best geometrical configuration.

It can be noticed that a significantly larger number of fitness function evaluations was achieved by the GA with a model area larger than that of the AIS and CAIS. Details are reported in Table 7.

The presented solutions met the natural frequency criterion for the first system mode; however, the AIS proposed a configuration with a smaller model area and used a smaller number of iterations than the GA. Moreover, the proposed novel costimulated artificial immune system's results reveal a similar solution in terms of the model area with a further benefit in the number of fitness function evaluations.

Table 6. Design variable comparison: genetic algorithm vs. artificial immune system.

Parameter Name	Genetic Algorithm (GA)	Artificial Immune System (AIS)	Costimulated Artificial Immune System (CAIS)
Casing shell A [in]	0.110	0.099	0.098
Casing shell B [in]	0.165	0.142	0.150
Casing shell C [in]	0.111	0.120	0.120
Forward hook thickness [in]	0.183	0.200	0.200
Rear hook thickness [in]	0.107	0.111	0.111
Forward hook leaning [°]	92.1	100.0	96.4
Rear hook leaning [°]	82.3	80.0	82.8
Nozzle shell thickness [in]	0.083	0.063	0.061
Forward hook position [in]	0.036	0.040	0.040
Rear hook position [in]	−0.048	−0.050	−0.050

Table 7. Algorithm solution comparison: genetic algorithm vs. artificial immune system.

	Genetic Algorithm (GA)	Artificial Immune System (AIS)	Costimulated Artificial Immune System (CAIS)
Number of fitness function evaluations	1374	443	380
Model area, in^2	19.163	19.109	19.114
Natural frequency	125.0	125.1	125.0

4. Discussion

The presented study confirms the application of artificial immune systems in optimization processes. It is suitable to support design selection where natural frequencies are important from a technical requirement perspective. The presented approach demonstrates data management between the AIS and Ansys Workbench based on session and CSV files to exchange information about the design parameters (input data) and measured characteristics (output data). The optimization process is based on a static metamodel. The AIS is not widely implemented in commercial engineering optimization packages compared the to GA. The CAIS variant brings the need to control the additional optimization parameters, which increase the setup complexity and pre-work time. Compared to commercial applications of the genetic algorithm, the AIS gives more beneficial results in terms of the model area and number of fitness function evaluations. Furthermore, the costimulated artificial immune system is more efficient in terms of the number of cases with a similar model area, as presented in Table 7, with the cost of a slightly poorer optimal design configuration.

Recommendations for further studies include the kinetic energy distribution in the parametric model definition and the incorporation of metamodel updates at each iteration, as well as additional benchmarking and back-to-back comparisons with other bio-inspired algorithms.

Author Contributions: Writing—original draft preparation, R.R.; writing—review and editing, M.S. and S.R. All authors have read and agreed to the published version of the manuscript.

Funding: This research received no external funding. The study was completed with the support of Avio Polska Sp. z o.o. (Grażyńskiego 141, 43-300 Bielsko-Biała, Poland), which provided the model, material data, boundary conditions and a shared workstation with an Ansys license.

Institutional Review Board Statement: Not applicable.

Informed Consent Statement: Not applicable.

Data Availability Statement: The data that support the findings of this study are not openly available due to reasons of sensitivity nature of the research.

Conflicts of Interest: Author Rafał Robak was employed by the company AvioPolska Sp. z o.o. The remaining authors declare that the research was conducted in the absence of any commercial or financial relationships that could be construed as a potential conflict of interest.

References

1. Geradin, M.; Rixen, D.J. *Mechanical Vibrations*; Wiley: Hoboken, NJ, USA, 2015.
2. Case, J.; Chilver, A.H. *Strength of Materials and Structures*; Edward Arnold: Baltimore, MD, USA, 1986.
3. Zienkiewicz, O.C. *The Finite Element Method in Structural and Continuum Mechanics*; McGraw-Hill: New York, NY, USA, 1971.
4. Flemming, S. Performance optimization of gas turbine engines using STUDGA. In Proceedings of the 14th Triennial World Congress, Beijing, China, 5–9 July 1999.
5. Davari, A.R.; Hasheminejad, M.; Boorboor, A. Shape Optimization of Wind Turbine Airfoils by Genetic Algorithm. *IACSIT Int. J. Eng. Technol.* **2013**, *5*, 206. [CrossRef]
6. Sandeep, S. A novel concept for non-linear multidisciplinary aerodynamic design optimization. *Aerosp. Sci. Technol.* **2017**, *70*, 626–635.
7. Cao, J.; Luo, Y.; Umar, B.M.; Wang, W.; Wang, Z. Influence of structural parameters on the modal characteristics of a Francis runner. *Eng. Fail. Anal.* **2022**, *131*, 105853. [CrossRef]
8. Robak, R.; Szczepanik, M.; Rulik, S. Parametric Optimization of Nozzle Turbine Vane Modal Characteristics by Means of Artificial System. *Appl. Sci.* **2022**, *12*, 9724. [CrossRef]
9. Hrehova, S.; Knapcikova, L. The Study of Machine Learning Assisted the Design of Selected Composites Properties. *Appl. Sci.* **2022**, *12*, 10863. [CrossRef]
10. Le, L.T.; Nguyen, H.; Dou, J.; Zhou, J. A Comparative Study of PSO-ANN, GA-ANN, ICA-ANN, and ABC-ANN in Estimating the Heating Load of Buildings' Energy Efficiency for Smart City Planning. *Appl. Sci.* **2019**, *9*, 2630. [CrossRef]
11. Burczyński, T.; Dlugosz, A.; Kus, W.; Orantek, P.; Poteralski, A.; Szczepanik, M.; Beluch, W. Intelligent computing in evolutionary optimal shaping of solids. In Proceedings of the 3rd International Conference on Computing, Communications and Control Technologies, Austin, TX, USA, 24–27 July 2005; Volume 3, pp. 294–298.
12. Grela, W. Optymalizacja Ewolucyjna Kształtu Łopatek Turbiny. Ph.D. Thesis, Silesian University of Technology, Gliwice, Poland, 2006.
13. Sawicki, W. *Histologia*; Wydawnictwo Lekarskie PZWL: Warsaw, Poland, 2003.
14. Wierzchoń, S.T. *Sztuczne Systemy Immunologiczne. Teoria i Zastosowania*; Akademicka Oficyna Wydawnicza EXIT: Warsaw, Poland, 2001.
15. Silva-Santos, C.H.; Goulart, P.R.; Bertelli, F.; Garcia, A.; Cheung, N. An artificial immune system algorithm applied to the solution of an inverse problem in unsteady inward solidification. *Adv. Eng. Softw.* **2018**, *121*, 178–187. [CrossRef]
16. Etaati, B.; Ghorrati, Z.; Ebadzadeh, M.M. A full-featured cooperative coevolutionary memory-based artificial immune system for dynamic optimization. *Appl. Soft Comput.* **2022**, *117*, 108389. [CrossRef]